

Prediction of Fracture Initiation in Hot Compression of Burn-Resistant Ti-35V-15Cr-0.3Si-0.1C Alloy

Saifei Zhang, Weidong Zeng, Dadi Zhou, and Yunjin Lai

(Submitted May 19, 2015; in revised form September 5, 2015; published online October 22, 2015)

An important concern in hot working of metals is whether the desired deformation can be accomplished without fracture of the material. This paper builds a fracture prediction model to predict fracture initiation in hot compression of a burn-resistant beta-stabilized titanium alloy Ti-35V-15Cr-0.3Si-0.1C using a combined approach of upsetting experiments, theoretical failure criteria and finite element (FE) simulation techniques. A series of isothermal compression experiments on cylindrical specimens were conducted in temperature range of 900–1150 °C, strain rate of 0.01–10 s⁻¹ first to obtain fracture samples and primary reduction data. Based on that, a comparison of eight commonly used theoretical failure criteria was made and Oh criterion was selected and coded into a subroutine. FE simulation of upsetting experiments on cylindrical specimens was then performed to determine the fracture threshold values of Oh criterion. By building a correlation between threshold values and the deforming parameters (temperature and strain rate, or Zener-Hollomon parameter), a new fracture prediction model based on Oh criterion was established. The new model shows an exponential decay relationship between threshold values and Zener-Hollomon parameter (Z), and the relative error of the model is less than 15%. This model was then applied successfully in the cogging of Ti-35V-15Cr-0.3Si-0.1C billet.

Keywords beta titanium alloy, FE simulation, fracture prediction, hot compression, Ti-35V-15Cr-0.3Si-0.1C

1. Introduction

Because traditional titanium and titanium alloys have a fatal weakness of their combustion sensitivity (Ref 1–4), burn-resistant titanium alloys have been developed to meet the special requirements of high-performance gas turbines that need not only excellent mechanical properties but also good burn resistance for some key parts. (Ref 5–7) In the early 1990s, Pratt and Whitney developed a commercial burn-resistant titanium alloy Ti-35V-15Cr, designated alloy C. (Ref 5) UK has developed a low-cost, burn-resistant beta alloy with a composition of Ti-25V-15Cr-2Al-0.2C in the late of 1990s (Ref 6). In the present study, Ti-35V-15Cr-0.3Si-0.1C is a new developed Ti-V-Cr series burn-resistant alloy based on the commercially-used alloy C. In order to achieve good burn-resistant properties, these alloys generally have very high content of alloy additions. As a result, a common feature of these alloys is their poor workability (Ref 8, 9). In our study, the cogging of Ti-35V-15Cr-0.3Si-0.1C is very difficult to perform due to frequent fracture issues.

It is well known that metal materials may undergo ductile fracture, which results from the progressive degradation of material stiffness, once plastic deformation reaches a certain limit. Ductile fracture is an irreversible process affecting the

workability (formability) of engineering materials. In industrial practice, the traditional trial-and-error methods may lead enormous costs when serious fracture occurs, and it is also quite time-consuming and very dependent on the engineers' experience. Therefore, the accurate prediction of a material's ductile fracture is of great practical importance in the design and optimization of processes and products.

There are a number of fracture models or criteria that have been developed to predict the initiation of fracture. These criteria may be classified into three categories as follows. The first are the empirical ones. The empirical criteria can either be strain-based or stress-based, in which fracture is presumed to occur when a strain or stress index reach a threshold. Typical empirical ones are Kuhn criterion (Ref 10) and Vujovic-Shabaik criterion (Ref 11). The second are semi-empirical criteria or cumulative plastic energy models, which consider the deforming process an energy accumulation, and fracture is presumed to occur when the accumulated energy reaches a certain value. In 1950, Freudenthal (Ref 12) proposed at the earliest in the view of energy that "Fracture will occur when the total plastic work per unit volume reaches some characteristic critical value." Cockcroft and Latham (Ref 13) built their model in 1968 based on the understanding that fracture in metal working process is dependent on maximum principal stress. Brozzo et al. (Ref 14) modified the Cockcroft-Latham criterion according to their own experimental results, considering the combine effect of maximum principal stress and hydrostatic pressure stress. Oh and Kobayashi (Ref 15) took the ratio of maximum principal stress to equivalent stress as the integral term and modified the Cockcroft-Latham criterion. The third category are micro/meso-scale damage models based on the observation of void initiation and growth followed by coalescence to form a crack. This is a completely different approach to formulate a fracture criterion. A mechanical analysis on void evolution in ductile metals started with McClintock's pioneering work (Ref 16). Hereafter, Rice and Tracey (Ref 17),

Saifei Zhang, Weidong Zeng, and Dadi Zhou, State Key Laboratory of Solidification Processing, Northwestern Polytechnical University, Xi'an 710072, China; and Yunjin Lai, Western Superconducting Technologies Co., Ltd., Xi'an 710018, China. Contact e-mails: zhsaifei@mail.nwpu.edu.cn and zengwd@nwpu.edu.cn.

Oyane (Ref 18) and Ayada et al. (Ref 19) developed various criteria adhering to this concept. It is worth mentioning that the porous plasticity model developed by Gurson (Ref 20) and the further modification by Tvergaard and Needleman (Ref 21, 22) is a great advance in the study of ductile fracture.

The advent of powerful numerical methods such as the technique of finite element method (FEM) to handle large deformation plasticity has made it possible to analyze the metalworking processes accurately. Thus, an integrated approach involving the workability experiments, theoretical failure criteria, and FEM technique emerged as a promising technique for accurate workability analysis. Kobayashi et al. (Ref 23) were one of the earliest to analyze ductile fracture in metal extrusion by combining McClintock and Cockcroft-Latham criteria with FEM technique. Since then, many researchers studied various aspects of the application of the computer-based numerical techniques to predict ductile fracture in a wide range of metalworking processes. Wifi et al. (Ref 24, 25) used the finite-element method extensively to evaluate various workability criteria in bulk forming processes. By designing various experiments and coding the criteria into FE model, Li et al. (Ref 26) studied the predicting reliability of several fracture criteria in diverse stress and strain states and fracture modes. Zhu et al. (Ref 27) adopt a new high-speed photography methodology to investigate the hot deformation process of Ti40 alloy and developed a fracture model using FEM technique. In the present study, in accordance with this strategy, hot compression experiments are conducted to determine the fracture threshold (critical fracture strain) in various conditions. A hot deformation fracture model which considers the effect of deforming temperature and strain rate is established to forecast the fracture initiation of Ti-35V-15Cr-0.3Si-0.1C alloy using a combined approach of theoretical failure criteria and FEM technique based on DEFORM-3D software and FORTRAN secondary development platform.

2. Material and Experimental Procedure

The nominal chemical composition of the alloy in the present investigation is Ti-35V-15Cr-0.3Si-0.1C (wt.%). It was provided by Western Superconducting Technologies Co., Ltd. (WST) in a partially processed ingot form. Ti-35V-15Cr-0.3Si-0.1C is a highly stabilized β titanium alloy since it has the highest molybdenum equivalency (47.5 wt.%) of all commercial β titanium alloys according to the 'moly equivalent' equation in Ref 28, which is used to indicate the beta stability of an alloy. The as-received microstructure of the material, as shown in Fig. 1, consists of coarse β grains and precipitates of titanium carbide (TiC_x , black dendrite in the OM).

In order to study the fracture behavior of Ti-35V-15Cr-0.3Si-0.1C in hot deformation, a series of isothermal compression tests were conducted on a computer-controlled Gleeble-1500 thermal simulator in the deformation temperature range from 900 to 1150°C with 50°C intervals, strain rate of 0.01, 0.1, 1, and 10 s⁻¹. The testing specimens from the billet were cylinders with 10 mm in diameter and 15 mm in height according to the standard method for hot compression test. A special high-temperature lubricant was coated on both ends of specimen, and tantalum foil with thickness of 0.1 mm was placed between die surface and specimen to prevent cementation. Samples were heated to the corresponding testing

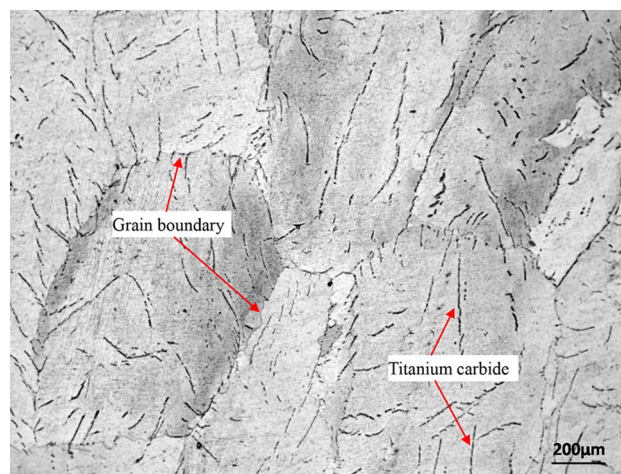


Fig. 1 Initial microstructure of the material in the as-received condition

temperatures with the rate of 10 °C/s and kept for 4 min before hot compression so as to obtain a uniform deformation temperature. Following the hot compression tests, each sample was air cooled, cleaned, measured, and visually inspected to determine the critical fracture reduction on the free surface. It is worth mentioning that bisection method was adopted in this study to determine the critical fracture reduction. The details of bisection method are seen in section 3.2.

By using the commercial finite element software DEFORM-3D, FEM simulations were conducted for each compression test to obtain data of the local stress-strain history and various damage parameters. In simulations, the material database was rebuilt, in which flow stress data were obtained from the isothermal compression tests to ensure the accuracy, and the thermo-physical parameters of this alloy were measured.

3. Experimental Results and Discussion

3.1 Fracture Behavior of Ti-35V-15Cr-0.3Si-0.1C

Understanding the fracture behavior is helpful to find out why the fracture occurs, which is an important basis of selecting and building the fracture model. Figure 2 is the photography of specimen deformed at 900-1150 °C/0.01-10 s⁻¹/70%. It is observed in the figure that cracks occur in 18 of all the 24 samples (below the red line), which reveals a poor workability of the present alloy. In addition, the tendency to cracking of this alloy increases with increasing strain rate and decreasing temperature. The effect of strain rate on cracking seems to be more significant. As for the fracture type of Ti-35V-15Cr-0.3Si-0.1C, there are generally three types that were observed. At low temperature and high strain rate such as 900 °C/10 s⁻¹, specimen exhibits 45° shear cracking throughout the whole specimen, as shown in Fig. 3(a). Metallographic examination of this sample reveals that the 45° shear cracking is associated with the intense flow instabilities caused by adiabatic shear bands (Fig. 3b), whereas at high temperature and high strain rate, the cracks always result from severe flow localization (Fig. 4, deformed at 1050 °C/10 s⁻¹). At low or moderate strain rate, the alloy displays the 'Z'-like cracking (Fig. 5a), which is attributed to

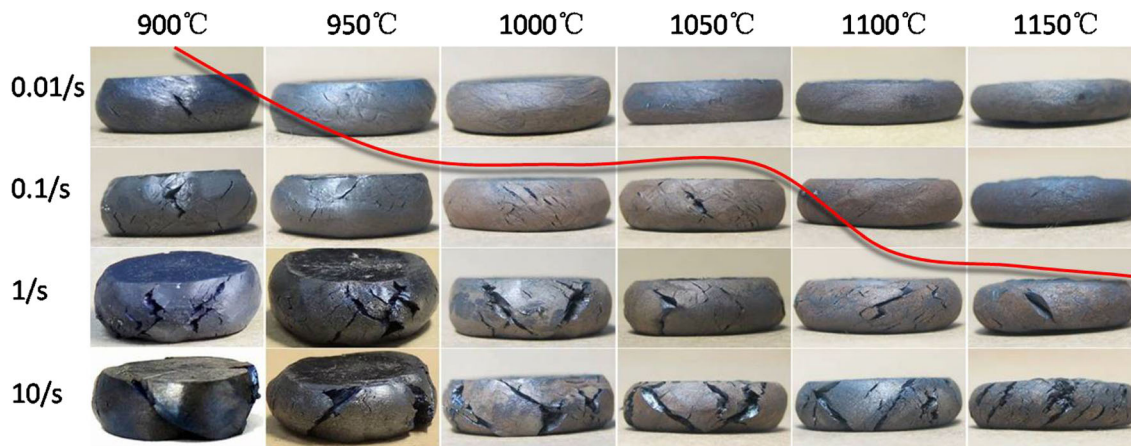


Fig. 2 The photography of specimen deformed at 900-1150 °C/0.01-10⁻¹

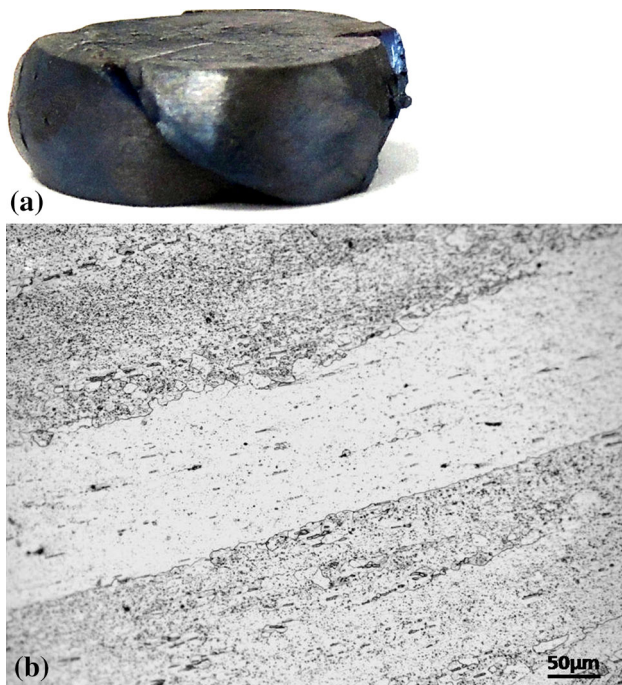


Fig. 3 A fracture sample at 900 °C/10⁻¹: (a) a 45° shear cracking cut throughout the whole specimen; (b) the proof of intense flow instabilities

the secondary tensile stresses caused by bulging of the cylindrical specimen during upsetting. Further SEM observation shows that the 'Z'-like free-surface cracking is a typical intergranular fracture (Fig. 5b). It seems that strain rate plays a most significant role in cracking and deformation non-uniformity. With the increase of strain rate, deformation non-uniformity increases. When samples are deformed at strain rate above 1 s⁻¹, flow localization occurs and deformation is localized in the middle area of samples. In cases of low temperature or large reduction, severe localized deformation would lead to cracking on the surface.

However, in spite of various fracture mechanisms observed, the macro-factors that affect crack initiation are the deforming conditions, i.e., temperature and strain rate. And close obser-

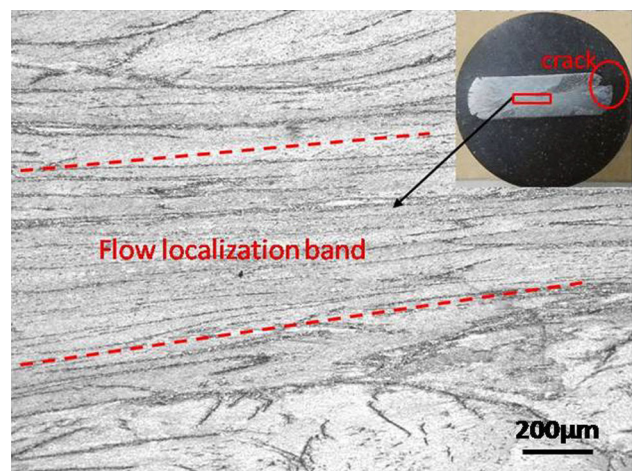


Fig. 4 A fracture sample deformed at 1050 °C/10⁻¹ shows severe flow localization

vation of the crack samples shows that cracking varies regularly with these two parameters if quantitative analyzed (see the next section), which provides a convenient way to model the fracture initiation without concerning too much about the detail mechanisms.

3.2 Determination of the Critical Fracture Reduction

To describe the cracking initiation quantitatively, Zeng (Ref 29), Zhu (Ref 27) used a term 'critical fracture strain' or 'critical fracture reduction,' namely, the maximum strain or height reduction that could be reached without the occurrence of cracks, to evaluate the hot workability of a certain alloy. Critical fracture reductions are basic experimental threshold data that can affect the accuracy of the final model. So it is significant to determine the critical fracture reduction accurately. There are several easy methods which can be employed to determine the critical fracture reduction such as acoustic emission (Ref 30, 31), infrared thermography (Ref 32), and high-speed photography (Ref 28), yet dichotomy or the bisection method (Ref 33), as a traditional method, is still the most reliable one though it needs to perform more experiments than the other methods. Therefore, dichotomy is adopted in the present

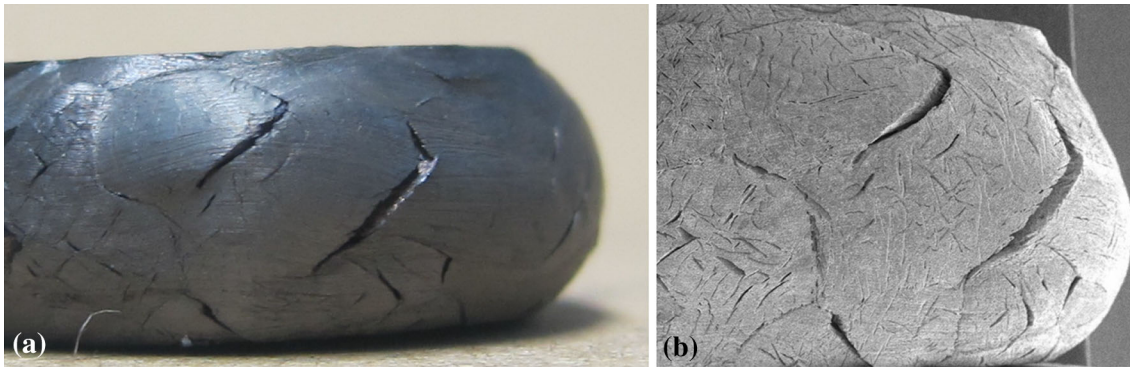


Fig. 5 A fracture sample reveals features of intergranular fracture

investigation to determine the critical fracture reduction. As is known, the critical fracture reduction under certain condition cannot be precisely predicted before compression test is conducted. However, by several experimental trials, we can get a reduction interval, in which the initial fracture occurs. The interval can then be narrowed by bisection method to a required accuracy, so the critical fracture reduction can thus be obtained. For instance, in one compression test, the specimen of 30% reduction does not crack, while the one of 50% cracks, then the reduction interval is 30-50%. According to the principal of bisection method, 40% reduction test will be added. If the specimen of 40% cracks, 35% test will be added further. By that analogy, testing continues until the desirable accuracy of critical fracture reduction (maximum = 5%) is reached.

Based on the above method, the critical fracture reduction in every deformation condition is obtained. The value of critical fracture reduction is plotted as a function of deformation temperature and strain rate in Fig. 6. It is seen from Fig. 6 that the critical fracture surface divides the 3-D deformation space into two zones, which are fracture zone above critical surface and safe zone below it, respectively. As expected, the critical fracture reduction has an increasing trend with the increasing of deformation temperature and decreasing of strain rate in the whole range of the experiment. In addition, the strain rate has a significant effect on the critical reduction. When samples are deformed at strain rate of 0.01 s^{-1} , the values of critical reduction at all testing temperatures are greater than 50%. While the strain rate rises to 10 s^{-1} , the critical reductions are all decreased below 35%. In fact, the workability of this alloy is so poor that cogging process is difficult to perform. The effect of strain rate and reduction on microstructure is limited by free surface fracture, which decreases the driving force of recrystallization (Ref 34). The poor workability can be attributed to the extremely high alloying effect and the coarse microstructure (very large beta grains and long brittle carbides). In practice, slow reduction speed is helpful for cogging but it reduces forging efficiency as well. Canned forging is thus recommended in order to increase efficiency and reduce cracking.

4. Modeling the Hot Deformation Fracture Criterion of Ti-35V-15Cr-0.3Si-0.1C

In the introduction section, various ductile fracture criteria are reviewed in categories and it is found that the existing

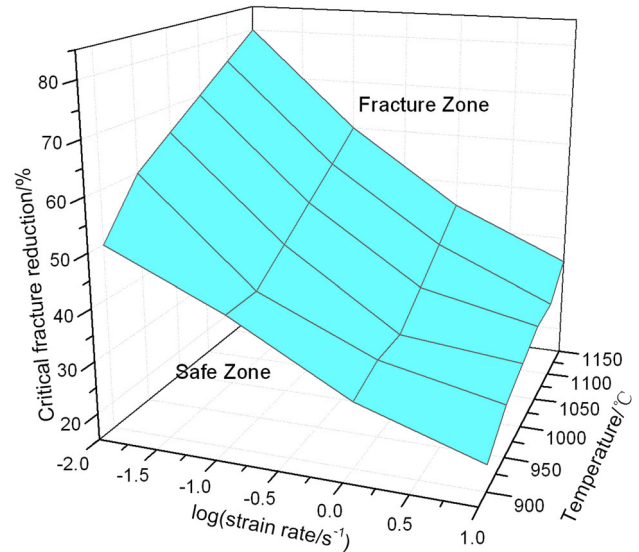


Fig. 6 Critical fracture reduction (C_f) plotted as a function of deformation temperature and strain rate

Table 1 Eight commonly used theoretical failure criteria and the corresponding formulas

Criteria	Formulas
Freudenthal	$C = \int_0^{\bar{\epsilon}_f} \bar{\sigma} d\epsilon$
Crookroft & Latham	$C = \int_0^{\bar{\epsilon}_f} \sigma^* d\epsilon$
Oh	$C = \int_0^{\bar{\epsilon}_f} \frac{\sigma^*}{\sigma} d\epsilon$
Brozzo	$C = \int_0^{\bar{\epsilon}_f} \frac{2\sigma_1}{3(\sigma_1 - \sigma_m)} d\epsilon$
Ayada	$C = \int_0^{\bar{\epsilon}_f} \frac{\sigma_m}{\sigma} d\epsilon$
Oyane	$C = \int_0^{\bar{\epsilon}_f} (1 + a \frac{\sigma_m}{\sigma}) d\epsilon$
Rice & Tracy	$C = \int_0^{\bar{\epsilon}_f} \exp(a \frac{\sigma_m}{\sigma}) d\epsilon$
Le Roy	$C = \int_0^{\bar{\epsilon}_f} (\sigma_1 - \sigma_m) d\epsilon$

criteria are developed on the basis of physical observation and micromechanical analysis of cold deformation. However, this work investigates the cracking during hot deformation process. One of the most important features that distinguish hot

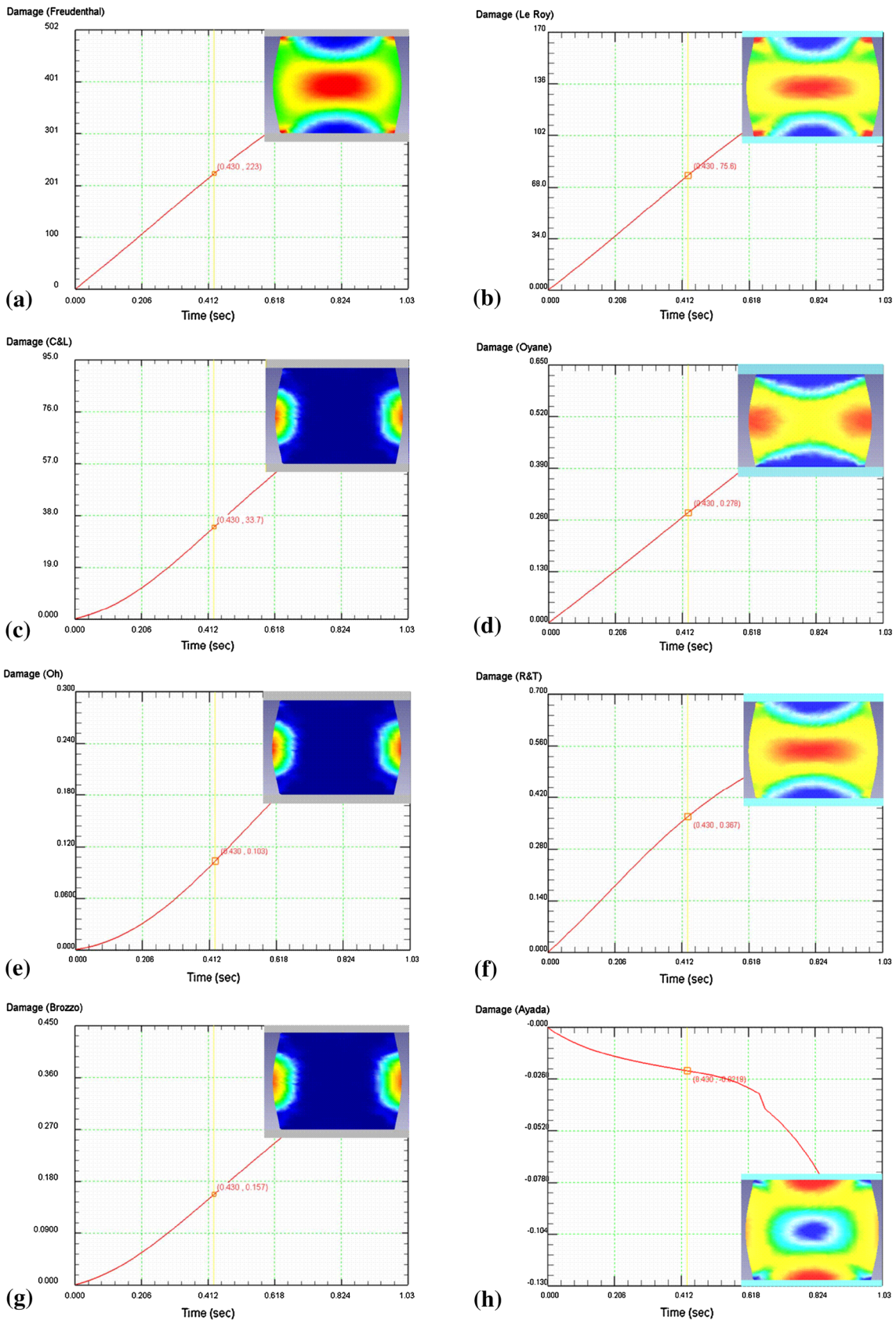


Fig. 7 Damage distribution based on eight criteria for specimen deformed at $1050\text{ }^{\circ}\text{C}/1\text{ s}^{-1}$: (a) Freudenthal criterion; (b) Le Roy criterion; (c) C&L criterion; (d) Oyane criterion; (e) R&T criterion; (f) Oh criterion; (g) Brozzo criterion; (h) Ayada criterion

deformation from cold one is that two parameters (deformation temperature and strain rate) play a key role in the thermally activated and restoration processes. And the analysis in section 3.2 section also reveals that critical fracture reduction is dependent on the deformation temperature and strain rate. Beyond that, whatever hot or cold deformation, one common element is that the initiation of ductile fracture depends strongly on the stress and strain-histories in metals, which is why many fracture criteria have the form that fracture occurs when the value of a damage parameter, given as integral form of stress and strain, reaches a threshold value. So for the sake of simplicity, our modeling strategy is as follows: first select a criterion from the commonly used criteria for cold deformation process; next is establishing fracture criterion for hot deformation by introducing the two parameters (temperature and strain rate) into the model.

To start with, the commonly used theoretical failure criteria for metalworking were chosen from the published literature as shown in Table 1. These criteria are in the form of damage accumulation formulated with an integral form of stress and strain in terms of certain macroscopic variables such as the equivalent stress, maximum principal stress and hydrostatic stress, that are most relevant to fracture initiation. The theoretical failure criteria listed in Table 1 were incorporated into FEM-based software Deform-3D by writing subroutines. Numerical experiments were then performed to simulate the physical laboratory compression tests on cylindrical specimens of Ti-35V-15Cr-0.3Si-0.1C alloy at $1050\text{ }^{\circ}\text{C}/1\text{ s}^{-1}$. Figure 7 shows the output damage distribution of specimen calculated by each criterion at the critical fracture reduction. The curves in Fig. 7 represent the variation of maximum damage values. As shown in Fig. 7, damage parameter calculated by Freudenthal and Le Roy criteria reaches its maximum value at the center and the corner of 45° direction of specimen. For Rice & Tracy criterion, the calculated maximum damage value is at the center of specimen. The maximum value by Ayada criterion is at the difficult deformation zone of specimen. Because upsetting deformation is characterized by compressive stress, the hydrostatic stress is negative value. And Ayada criterion is in an integral form of hydrostatic stress and strain. Therefore, damage value calculated by Ayada criterion is negative. The rest four criteria show a similar output: the maximum damage value is at the equator on free surface bulge of cylindrical

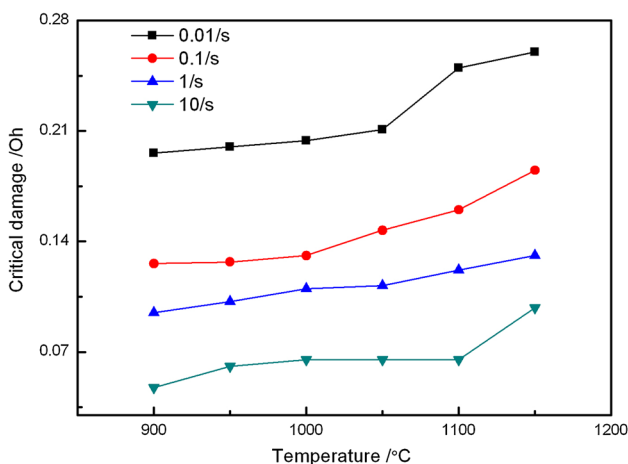


Fig. 8 The variation of critical damage value calculated by Oh criterion with different deforming conditions

specimen. According to the definition of fracture criteria, damage value calculated by a criterion is expected to get its maximum at the fracture location and the maximum value is thus called threshold value or critical damage value. In section 3.1, the observation of crack specimens show that the fracture location is at the equator on free surface bulge, so the four criteria, i.e., Freudenthal criterion, Le Roy criterion, Rice & Tracy criterion and Ayada criterion, are regarded as inappropriate for modeling the hot deformation fracture criterion of Ti-35V-15Cr-0.3Si-0.1C.

In order to further select one criterion from the rest four (Crockroft & Latham, Oh, Brozzo, Oyane), more numerical experiments in various deforming conditions were conducted and the threshold values attained by each of the four criteria were extracted and analyzed. Figure 8 shows the variation of

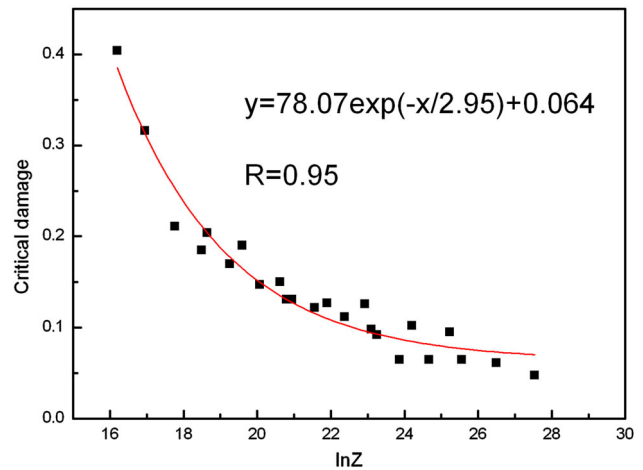


Fig. 9 The established relationship between critical damage and Zener-Hollomon parameter by exponential decay model

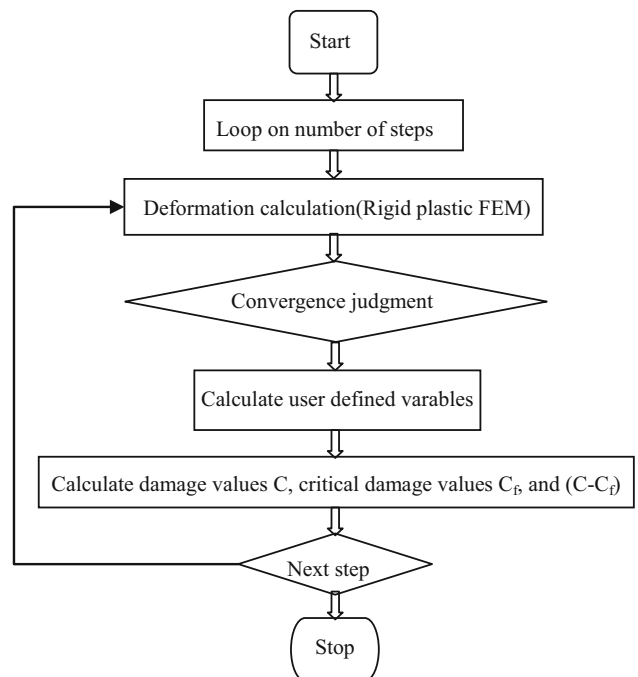


Fig. 10 The flow chart of FE program including user subroutine

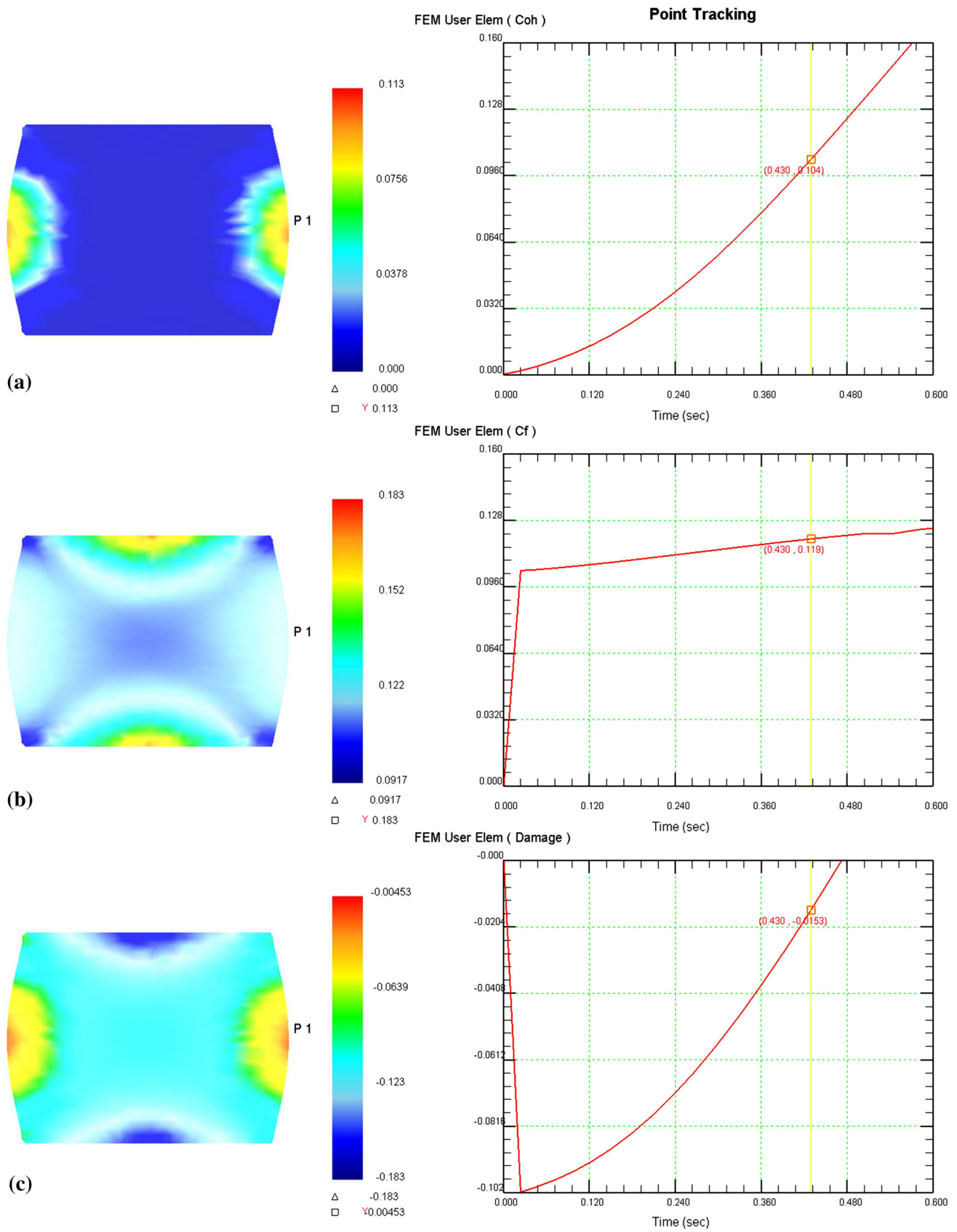


Fig. 11 Test and verification of the new prediction model

threshold values calculated by Oh criterion with deformation temperatures and strain rates. As can be seen in the figure, the threshold values rise with the increase of deformation temperature and the decrease of strain rate. This is consistent with the result of laboratory compression tests. Because the workability is better at higher temperature and lower strain rate, threshold values can reach a relatively high level before fracture occurs. So Oh criterion is suitable for modeling the hot deformation fracture criterion of Ti-35V-15Cr-0.3Si-0.1C.

Since there is a correlation between threshold values and the deforming parameters (temperature and strain rate), the new fracture model based on Oh criterion might be written in the following form:

$$\int_0^{\bar{\epsilon}_f} \frac{\sigma^*}{\bar{\sigma}} d\epsilon = C_f = f(T, \dot{\epsilon}) \quad (\text{Eq 1})$$

In equation (1), $\bar{\epsilon}_f$ is the effective strain when initial fracture occurs; σ^* is the maximum principal stress; $\bar{\sigma}$ is the effective stress; C_f is the threshold value of Oh criterion; T is the deformation temperature and $\dot{\epsilon}$ is the strain rate. The strain rate and deformation temperature are often incorporated into a single parameter: the Zener-Hollomon parameter (Z), which is defined as $Z = \dot{\epsilon} \exp(\frac{Q}{RT})$, where $\dot{\epsilon}$ is the strain rate, Q is the activation energy, R is the ideal gas constant, and T is the absolute temperature. Since Z parameter represents a combined effect of strain rate and temperature, it is appropriate to introduce Z parameter to replace the two parameters (temperature and strain rate).

Figure 9 shows the relationship between Zener-Hollomon parameter ($\ln Z$) and the threshold value (C_f) of Oh criterion. As can be seen, C_f decays exponentially with $\ln Z$ increasing. The correlation coefficient (R) is 0.95, demonstrating that the built relationship is valid. Meanwhile, the correlation of $\ln Z$ and C_f suggests that the ductile fracture is not only dependent on the stress and strain, but also on the combined effect of temperature and strain rate in hot forming. Thus, the ductile fracture model of hot deformation in the basis of Oh criterion was established as follows:

$$\int_0^{\bar{\epsilon}_f} \frac{\sigma^*}{\bar{\sigma}} d\epsilon > 78.073 \exp\left(-\frac{\ln Z}{2.949}\right) + 0.0635 \quad (\text{Eq 2})$$

If the state of a location in metals meets the above relationship during hot deformation, it can be assumed that fracture will occur at this location.

The new fracture model based on Oh criterion (Eq 2) was then coded into a subroutine using FORTRAN language, and inserted the subroutine in the sequence of FE calculating operations. The flow chart of FE program including user subroutine is shown in Fig. 10. Cracking is supposed to occur when $C - C_f > 0$. By doing this, the prediction of initial fracture location and critical fracture strain can be achieved. For the purpose of testing and verifying the new model, the comparison of initial fracture location and critical fracture reduction between the experimental and predicted values for the upsetting of Ti-35V-15Cr-0.3Si-0.1C has been conducted. As can be seen in Fig. 11, the predicted maximum damage value is at the equator on free surface bulge, which is consistent with experimental results. Point P1 is picked at the equator. The damage value of P1 attained by Oh criterion and new fracture model at 35% reduction is 0.104 (Fig. 11a) and -0.015 (Fig. 11c), respectively. Figure 11(b) shows the threshold value in this condition is 0.119, which is the difference between 0.104 and -0.015 , demonstrating that FE subroutine is running cor-

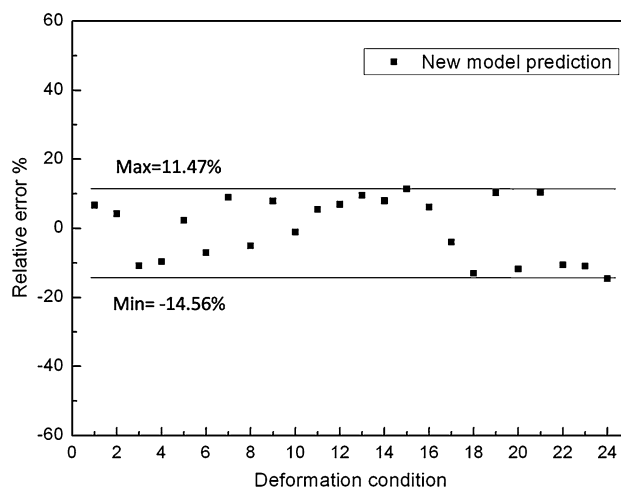


Fig. 12 Relative error of the initial fracture reduction by new model prediction

rectly in the main program loop. In addition, because the damage value of P1 predicted by new fracture model is negative (-0.015), no crack is supposed to occur at point P1 at this reduction (35%) theoretically. The damage value of P1 turns positive (0.009) when reduction rises to 37%, which means that the critical fracture reduction predicted by new criterion is 35-37%. Considering the experimental critical fracture reduction is 35%, the relative error is less than 5.7%. Simulation results in other deforming conditions (Fig. 12) show that the maximum and minimum relative errors of new criterion are 11.47 and -14.56% , respectively. Therefore, the fracture prediction model using a combined approach of theoretical failure criteria and FEM technique is reliable.

5. Application of the fracture prediction model in the cogging of Ti-35V-15Cr-0.3Si-0.1C billet

As mentioned previously, the cogging process of Ti-35V-15Cr-0.3Si-0.1C is difficult to control due to the poor workability of the material. The traditional trial-and-error method not only increases cost but also prolongs production time. In order to precisely predict the possible cracking during deformation, a new fracture model has been built in section 4 to predict the fracture initiation. In the present section, the prediction model is going to be applied in the cogging process of Ti-35V-15Cr-0.3Si-0.1C billet so as to optimize processing parameters as well as to further test the prediction model.

In industrial application, the billet ($210 \times 250 \times 780$ mm) will be forged into a thick plate that will be used to make engine cases, in which the process of drawing out is of central importance. Therefore, simulation on drawing out is conducted to predict the possible cracking during the process. Simulation results on different reductions (20-50%, 1050 °C, 10 mm/s), loading speeds (5-35 mm/s, 1050 °C, 40%), deforming temperatures (900-1100 °C, 10 mm/s, 40%) are shown in Fig. 13, 14, and 15, respectively. As indicated in the color bar on the right of the figures, blue color in the billet represents area in which the damage value $C - C_f \leq 0$, namely, the safe area. Other colors are the predicted unsafe area ($C - C_f \geq 0$), where surface cracking might take place. As shown in Fig. 13, the effect of

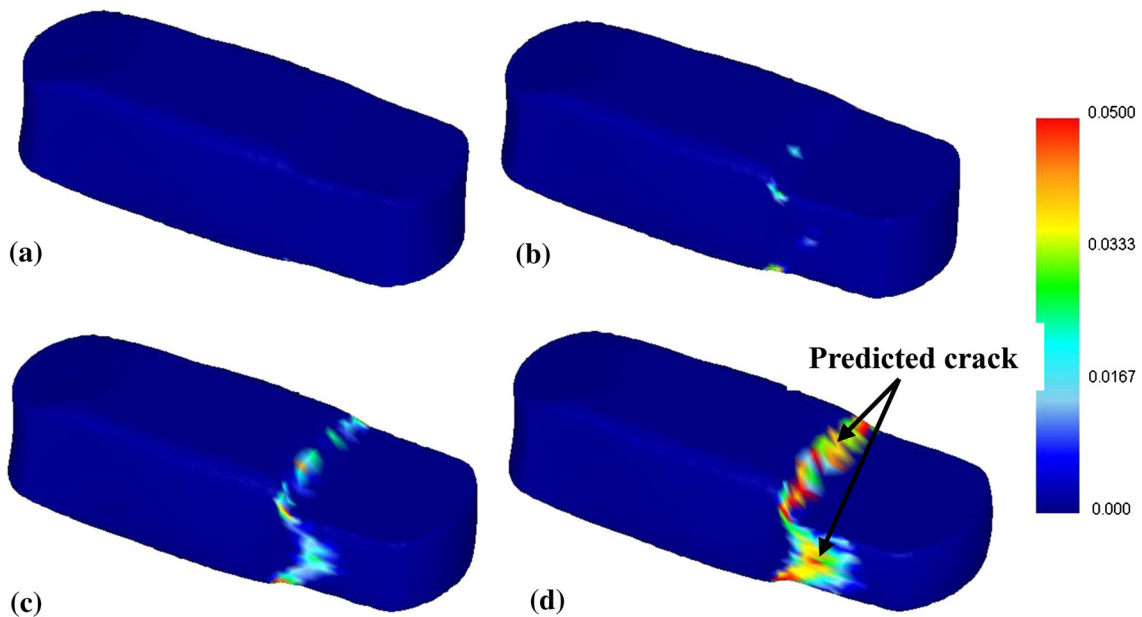


Fig. 13 The damage value distribution predicted by fracture criterion at different reductions: (a) 20%; (b) 30%; (c) 40%; (d) 50%

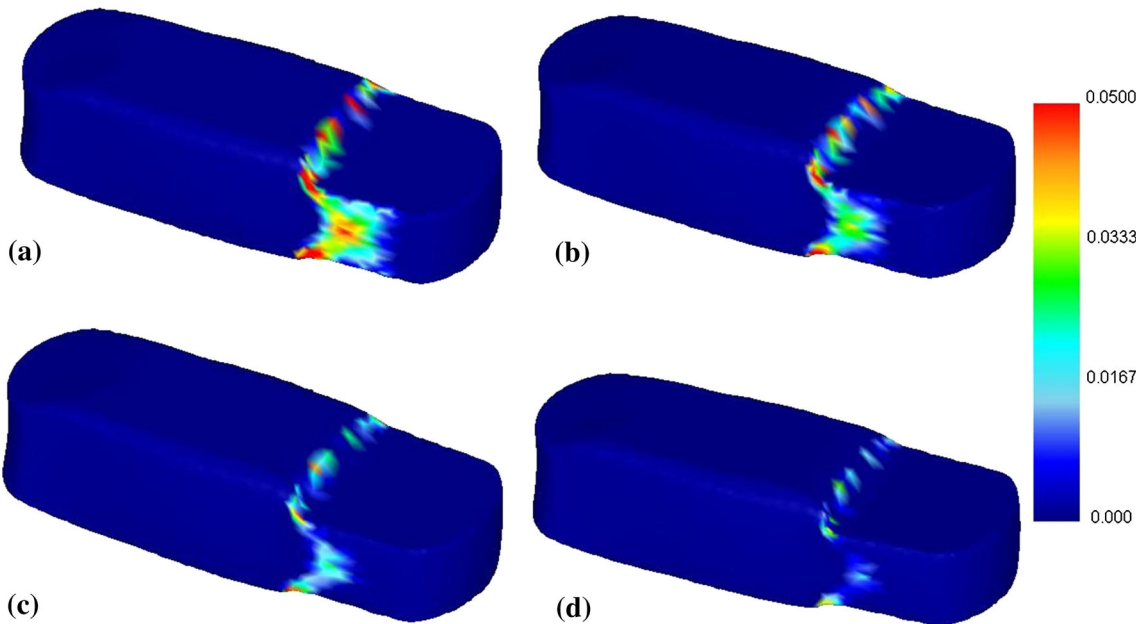


Fig. 14 The damage value distribution predicted by fracture criterion at different starting temperatures: (a) 900 °C; (b) 1000 °C; (c) 1050 °C; (d) 1100 °C

reduction on the distribution of damage value is significant. The unsafe area increases with the reduction increasing, as well as the maximum damage value does. This implies that cracking gets severer at larger reductions. It is noted that no obvious cracking occurs when the reduction is no more than 30% (Fig. 13b). In addition, the location of possible cracking is more likely to be the following two sites: the first is at the round corner of contact area between die and billet, and the next is on free surface bulge of the billet. Figure 14 is the distribution of damage value predicted by fracture criterion at different loading speeds. As expected, the degree of cracking is higher at higher loading speed. In this speed range, the average strain rate is

about $0.02\text{--}0.3\text{ s}^{-1}$. The effect of loading speed on cracking is the same as that of strain rate when compared with the previous compression test. Moreover, it is seen in Fig. 14 that cracking occurs in all the four conditions, which means that the reduction of 40% is too large for the process. Deforming temperature shows an opposite effect on cracking, as shown in Fig. 15, i.e., cracking decreases with increasing temperature. In order to avoid cracking and increase the efficiency of drawing out, processing parameters should be in the range of 1050–1100 °C, 10 mm/s, 30% at one reduction according to the simulation results. As a validation test, a thick plate has been successfully forged using the optimized parameters (see in

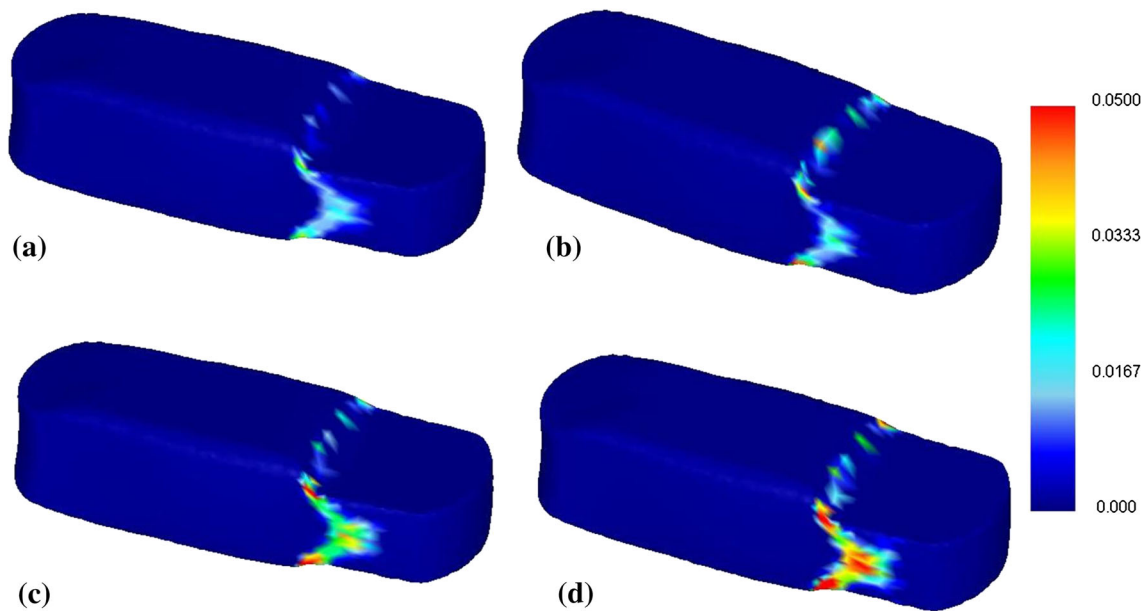


Fig. 15 The damage value distribution predicted by fracture criterion at loading speeds: (a) 5 mm/s; (b) 10 mm/s; (c) 20 mm/s; (d) 35 mm/s



Fig. 16 The thick plate of Ti-35V-15Cr-0.3Si-0.1C forged using the optimized parameters

Fig. 16), which further proves the validity of the fracture prediction model established in section 4 (Eq 2).

6. Conclusions

Based on the upsetting experiments, theoretical failure criteria, finite element (FE) simulation and secondary development techniques, a fracture prediction model which considers the effect of stress state, strain history, hot deformation parameters (strain rate and temperature) on fracture in hot compression of Ti-35V-15Cr-0.3Si-0.1C alloy has been established successfully in this study. The main conclusions of the present research are as follows:

- (1) Compression experiments on cylindrical specimens show a very poor workability of Ti-35V-15Cr-0.3Si-0.1C alloy. Frequent cracks are found during deformation and the analysis of crack samples reveals that shearing fracture, severe flow localization, and intergranular fracture are three mechanisms responsible for macro-failure.
- (2) Critical fracture reduction is dependent on the deforming temperature and strain rate. Critical fracture reduction increases with the increasing of deformation temperature

and decreasing of strain rate in the whole range of the experiment.

- (3) The new model shows an exponential decay relationship between threshold values and Zener-Hollomon parameter (Z). This model can effectively forecast the fracture initiation over a wide range of deforming temperature and strain rate during the compression of Ti-35V-15Cr-0.3Si-0.1C alloy. This model has been successfully applied in the cogging process.

Acknowledgments

This work was supported by the National Natural Science Foundation of China with Grant No. 51075333.

References

1. E.A. Borisova and K.V. Bardanov, Ignition of Titanium Alloys in Media Containing Oxygen, *Met. Sci. Heat Treat.*, 1963, 5(2), p 98–101
2. V.I. Deryabina, N.N. Kolgatin, O.P. Luk'yanov et al., The Ignition of a Low-Alloy Titanium α -Alloy During Fracture in an Oxygen-Containing Atmosphere, *Mater. Sci.*, 1973, 7(1), p 14–17

3. V.I. Bolobov, Deflagration of Titanium in an Oxygen Flow, *Combustion, Explosion and Shock Waves*, 1993, **29**(2), p 138–141
4. V.I. Bolobov, Possible Mechanism of Autoignition of Titanium Alloys in Oxygen, *Combustion, Explosion and Shock Waves*, 2003, **39**(6), p 677–680
5. D.M. Berczik, Age Hardenable Beta Titanium Alloy: U.S. Patent 5,176,762. 1993-1-5
6. Y.G. Li, P.A. Blenkinsop, M.H. Loretto et al., Effect of Carbon and Oxygen on Microstructure and Mechanical Properties of Ti-25V-15Cr-2Al Alloys, *Acta Mater.*, 1999, **47**(10), p 2889–2905
7. Y.Q. Zhao, K.Y. Zhu, X.M. Zhao, A Ti-V-Cr series Burn Resistant Titanium Alloy. 1997. (in Chinese)
8. P.A. Russo, S.R. Seagle, in *Proceedings of 8th World Conference on 'Titanium'*, (ed. P. A. Blenkinsop et al.), pp. 841–847; 1996, London, The Institute of Materials
9. X.M. Zhang, W.D. Zeng, and Y. Shu, Fracture Criterion for Predicting Surface Cracking of Ti40 Alloy in Hot Forming Processes, *Trans. Nonferr. Met. Soc. China*, 2009, **19**(2), p 267–271
10. H.A. Kuhn, P.W. Lee, and T. Erturk, A Fracture Criterion for Cold Forming, *J. Eng. Mater. Technol.*, 1973, **95**(4), p 213–218
11. V. Vujovic and A.H. Shabaik, A New Workability Criterion for Ductile Metals, *J. Eng. Mater. Technol.*, 1986, **108**(3), p 245–249
12. A.M. Freudenthal, *The Inelastic Behavior of Engineering Materials and Structures*, John Wiley and Sons, New York, 1950, p 1–70
13. M.G. Cockcroft and D.J. Latham, A Simple Criterion of Fracture for Ductile Metals, *J. Inst. Met.*, 1968, **96**, p 33–39
14. P. Brozzo, B. Deluca, R. Rendina, A new method for the prediction of formability limits in metal sheets. in *Proc. 7th biennial Conf. IDDR* (1972)
15. S.I. Oh, C.C. Chen, and S. Kobayashi, Ductile Fracture in Axisymmetric Extrusion and Drawing-Part 2: Workability in Extrusion and Drawing, *J. Manuf. Sci. Eng.*, 1979, **101**(1), p 36–44
16. F.A. McClintock, Challenges in Fracture Mechanics, *Dev. Mech.*, 1969, **5**, p 905–919
17. J.R. Rice and D.M. Tracey, On the Ductile Enlargement of Voids in Triaxial Stress Fields, *J. Mech. Phys. Solids*, 1969, **17**(3), p 201–217
18. M. Oyane, Criteria of Ductile Fracture Strain, *Bull. JSME*, 1972, **15**(90), p 1507–1513
19. M. Ayada, T. Higashino, and K. Mori, Central Bursting in Extrusion of Inhomogeneous Materials, *Adv. Technol. Plast.*, 1987, **1**, p 553–558
20. A.L. Gurson, Continuum Theory of Ductile Rupture by Void Nucleation and Growth: Part I: Yield Criteria and Flow Rules for Porous Ductile Media, *J. Eng. Mater. Technol.*, 1977, **99**(1), p 2–15
21. V. Tvergaard, A. Needleman, and K.K. Lo, Flow Localization in the Plane Strain Tensile Test, *J. Mech. Phys. Solids*, 1981, **29**(2), p 115–142
22. A. Needleman and J.R. Rice, *Limits to Ductility set by Plastic Flow Localization*, Springer, New York, 1978, p 237–267
23. S. Kobayashi, C.H. Lee, Deformation mechanics and workability in upsetting solid circular cylinders, in *Proceedings of the North American Metalworking Research Conference* vol. 1 (1973)
24. A.S. Wifi, N. El-Abbasi, and A. Abdel-Hamid, A Study of Workability Criteria in Bulk Forming Processes, *Stud. Appl. Mech.*, 1995, **43**, p 333–357
25. A.S. Wifi, A. Abdel-Hamid, and N. El-Abbasi, Computer-Aided Evaluation of Workability in Bulk Forming Processes, *J. Mater. Process. Technol.*, 1998, **77**(1), p 285–293
26. H. Li, M.W. Fu, J. Lu et al., Ductile Fracture: Experiments and Computations, *Int. J. Plast.*, 2011, **27**(2), p 147–180
27. Y. Zhu, W. Zeng, F. Zhang et al., A New Methodology for Prediction of Fracture Initiation in Hot Compression of Ti40 Titanium Alloy, *Mater. Sci. Eng. A*, 2012, **553**, p 112–118
28. P.J. Bania, Beta Titanium Alloys and Their Role in the Titanium Industry, *JOM*, 1994, **46**(7), p 16–19
29. W.D. Zeng, Y. Shu, X.M. Zhang et al., Hot Workability and Microstructure Evolution of Highly β Stabilised Ti-25V-15Cr-0.3Si Alloy, *Mater. Sci. Technol.*, 2008, **24**(10), p 1222–1229
30. O. Andreykiv, V. Skalsky, O. Serhiyenko et al., Acoustic Emission Estimation of Crack Formation in Aluminium Alloys, *Eng. Fract. Mech.*, 2010, **77**(5), p 759–767
31. C.K. Mukhopadhyay, T. Jayakumar, T.K. Haneef et al., Use of Acoustic Emission and Ultrasonic Techniques for Monitoring Crack Initiation/Growth During Ratcheting Studies on 304LN Stainless Steel Straight Pipe, *Int. J. Press. Vessels Pip.*, 2014, **116**, p 27–36
32. S. Punnose, A. Mukhopadhyay, R. Sarkar et al., Determination of Critical Strain for Rapid Crack Growth During Tensile Deformation in Aluminide Coated Near- α Titanium Alloy Using Infrared Thermography, *Mater. Sci. Eng. A*, 2013, **576**, p 217–221
33. Y. Shu, W. Zeng, X. Zhang et al., Fracture Predicting of Ti40 Burn Resistant Titanium Alloy in Hot Forming, *Rare Met. Mater. Eng.*, 2006, **35**(12), p 1900–1903
34. R.D. Doherty, D.A. Hughes, F.J. Humphreys et al., Current Issues in Recrystallization: A Review, *Mater. Sci. Eng. A*, 1997, **238**(2), p 219–274